AD-A152 917 LOW VOLTAGE FREE ELECTRON LASER DEVELOPMENT(U) HUGHES RESEARCH LABS MALIBU CA R J HARVEY ET AL. FEB 85 N00014-82-C-0220 1/1

UNCLASSIFIED F/G 20/5 NL

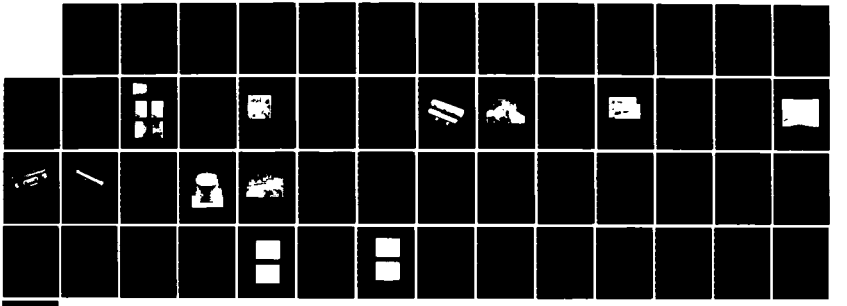

END

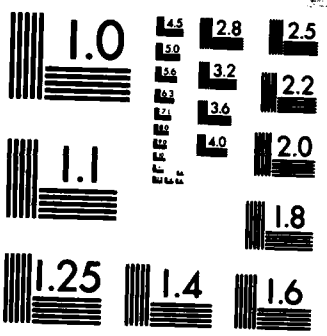

(12)

LOW VOLTAGE FREE ELECTRON LASER DEVELOPMENT

R.J. Harvey and F.A. Dolezal

Hughes Research Laboratories
3011 Malibu Canyon Road
Malibu, CA 90265

February 1985

N00014-82-C-0220
Final Report
1 February 1982 through 31 October 1984

OFFICE OF NAVAL RESEARCH
800 N. Quincy Street
Arlington, VA 22217

REPORT DOCUMENTATION PAGE

1a. REPORT SECURITY CLASSIFICATION UNCLASSIFIED	1b. RESTRICTIVE MARKINGS
2a. SECURITY CLASSIFICATION AUTHORITY	3. DISTRIBUTION/AVAILABILITY OF REPORT
2b. DECLASSIFICATION/DOWNGRADING SCHEDULE	
4. PERFORMING ORGANIZATION REPORT NUMBER(S)	5. MONITORING ORGANIZATION REPORT NUMBER(S)
6a. NAME OF PERFORMING ORGANIZATION Hughes Research Laboratories 6b. OFFICE SYMBOL (If applicable) 30-00	7a. NAME OF MONITORING ORGANIZATION OFFICE OF NAVAL RESEARCH
6c. ADDRESS (City, State and ZIP Code) 3011 Malibu Canyon Road Malibu, CA 90265	7b. ADDRESS (City, State and ZIP Code) 1030 Green Street Pasadena, CA
8a. NAME OF FUNDING/SPONSORING ORGANIZATION OFFICE OF NAVAL RESEARCH 8b. OFFICE SYMBOL (If applicable)	9. PROCUREMENT INSTRUMENT IDENTIFICATION NUMBER N00014-82-C-0220
8c. ADDRESS (City, State and ZIP Code) 800 N. Quincy Street Arlington, VA 22217	10. SOURCE OF FUNDING NOS. PROGRAM ELEMENT NO. / PROJECT NO. / TASK NO. / WORK UNIT NO.
11. TITLE (Include Security Classification) LOW VOLTAGE FREE ELECTRON LASER DEVELOPMENT	
12. PERSONAL AUTHOR(S) Robin J. Harvey and Frank A. Dolezal	
13a. TYPE OF REPORT Final Report 13b. TIME COVERED FROM 2/1/82 TO 10/31/84	14. DATE OF REPORT (Yr., Mo., Day) February 1985 15. PAGE COUNT
16. SUPPLEMENTARY NOTATION	
17. COSATI CODES FIELD / GROUP / SUB. GR.	18. SUBJECT TERMS (Continue on reverse if necessary and identify by block number)

19. ABSTRACT (Continue on reverse if necessary and identify by block number)

The two-beam, two-stage Free Electron Laser (FEL)[1] offers the possibility of a compact, low voltage FEL (LVFEL). This LVFEL development program has addressed the issues of the first stage of such a LVFEL. During the course of this program we have demonstrated the first plane-polarized mm-wave FEL oscillator. The FEL operates at 31 GHz with an output power of 60 kW. We have observed radiation on the forward- and backward-wave portions of the dispersion curve. The gain of the device has been estimated, from the signal buildup time, to be approximately 5% for both forward- and backward-wave operation. The linewidth of this device has been measured in the forward-wave mode to be 1.7% in voltage space and <4.8% in frequency space. These linewidths correspond well to theoretically predicted values of 3.1 and 3.7%, respectively. The polarization of the device has been measured to be roughly perpendicular to the direction of the wiggler field.

20. DISTRIBUTION/AVAILABILITY OF ABSTRACT UNCLASSIFIED/UNLIMITED ☐ SAME AS RPT. ☐ DTIC USERS ☐	21. ABSTRACT SECURITY CLASSIFICATION Unclassified
22a. NAME OF RESPONSIBLE INDIVIDUAL R.E. Behringer	22b. TELEPHONE NUMBER (Include Area Code) (818) 795-5971 22c. OFFICE SYMBOL

DD FORM 1473, 83 APR EDITION OF 1 JAN 73 IS OBSOLETE.

TABLE OF CONTENTS

LIST OF ILLUSTRATIONS

SECTION 1

INTRODUCTION

The two-beam, two-stage Free Electron Laser (FEL)[1] offers the possibility of a compact, low-voltage FEL (LVFEL). This LVFEL development program has addressed the issues of the first stage of such a LVFEL. During the course of this program we have demonstrated the first plane-polarized mm-wave FEL oscillator. The FEL operates at 31 GHz with an output power of 60 kW. We have observed radiation on the forward- and backward-wave portions of the dispersion curve. The gain of the device has been estimated, from the signal buildup time, to be approximately 5% for both forward- and backward-wave operation. The linewidth of this device has been measured in the forward-wave mode to be 1.7% in voltage space and <4.8% in frequency space. These linewidths correspond well to theoretically predicted values of 3.1 and 3.7%, respectively. The polarization of the device has been measured to be roughly perpendicular to the direction of the wiggler field.

The evolution of the FEL has reached the point at which devices are being reported in operation all the way from microwave frequencies to that of visible light[2]. The physics community is eagerly awaiting the availability of the new tunable, far-infrared FEL now being developed at the University of California at Santa Barbara (UCSB) which will open up a new era in the study of materials. Eventually, the FEL will be able to vary the frequency of a high-power-IR beam through previously unreachable regions of the infrared spectrum where a detailed knowledge of the phonon spectrum is of crucial importance to advancements in solid-state physics. In order to cover the frequency band up to the near infrared, the present UCSB 400-μm, single-stage FEL must be modified to function as a two-stage FEL. The present program is directed toward this end.

Availability of a frequency-agile, two-band (e.g., mm-wave and IR) source will impact a broad range of scientific as well as military needs. A two-beam, two-stage FEL is made up of two independent E-beams, as shown in Figure 1. Each stage corresponds to one E-beam line and an interaction region. The pump field for the first stage is a static, spatially-periodic magnetic field called a "wiggler" or wiggler magnet. The pump field for the second stage is provided by an electromagnetic standing wave which is generated in the first stage. The primary function of the wiggler is to induce transverse oscillation of the beam. It is this transverse motion of the electrons which is able to couple energy to an electromagnetic (or signal) wave. The electron beam is unstable in the presence of both the signal wave and the wiggler field because of an average (i.e., pondermotive) force on the electrons. The periodic field of the wiggler and the signal wave form an electromagnetic beat wave which propagates at the velocity of the electron beam. The net effect is to first bunch the electrons at the nodes of the beat wave which then forces the electron bunches to oscillate coherently as they pass through the wiggler. These effects result in system gain. Furthermore, due to the nature of the relativistic Doppler effect, the signal wavelength is shorter than the wiggler period, decreasing quadratically with E-beam energy.

The frequency shift of the two-stage FEL is proportional to the product of the shifts from each stage; i.e., proportional to $2\gamma_1^2 \cdot 4\gamma_2^2$, where γ is the relativistic mass factor. It is for this reason that a two-stage FEL is able to operate at a lower voltage than single-stage devices for a given output frequency.

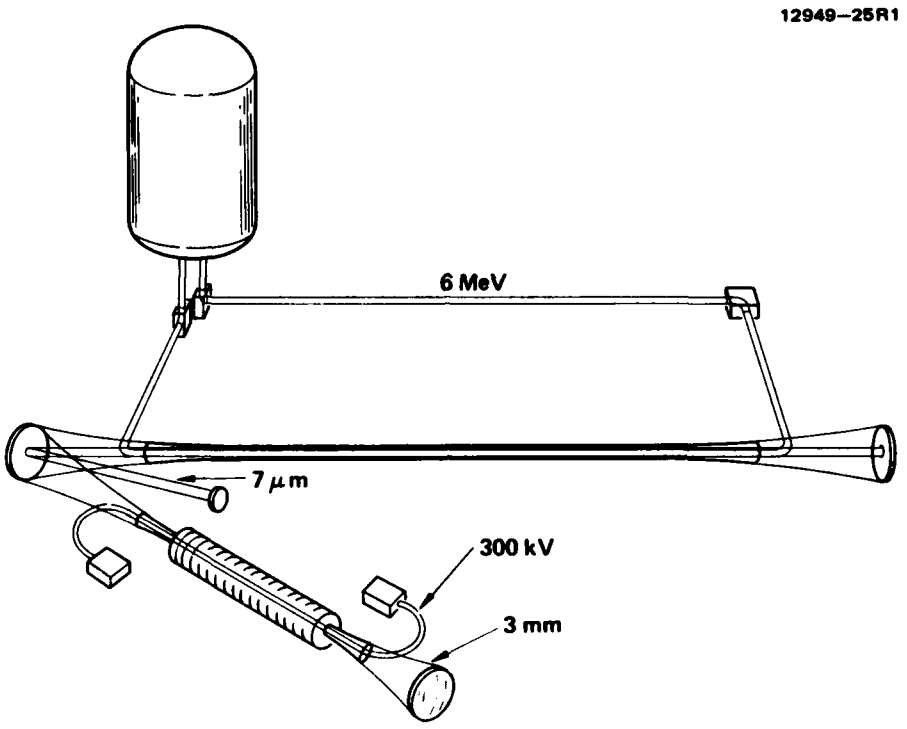

Figure 1. Two-stage, two-beam FEL concept.

As in all two-stage FELs,[3] the second-stage-pump signal must have a high intensity in order for sufficient bunching to occur. The present program is focused on understanding how to achieve high power operation of the first stage and on the parameterization of the device in preparation for implementation in a complete LVFEL system.

SECTION 2

EXPERIMENTAL APPARATUS DETAILS

The principal components of the FEL oscillator are shown in Figure 2. The apparatus is designed to make full use of a low emittance E-beam as opposed to the practice of using only the lower-emittance center of a much higher current beam, the normal practice in most other low current mm-wave FEL experiments. The 5- to 15-A E-beam is injected at 100 to 300 kV into a weak (400-G) guidefield. A quadrature detector is located at the solenoid input for beam centering. The guidefield directs the beam into the high-Q cavity and wiggler assembly. Previous experiments[4] have used a depressed collector, resulting in collection efficiencies of 94%. However, a depressed collector was not used in the present experiments; the beam was dumped on the solenoid walls and elsewhere. The E-gun cathode operates at ground potential and the anode, solenoidal guidefield, and wiggler magnet are operated at high voltage.

The overall experimental arrangement is shown in Figure 3. The FEL components are housed in a high vacuum chamber which is pumped to a vacuum of 10^{-7} Torr or better. The system power is provided through a step-up transformer and a tuned, pulse-forming network. All controls are connected to the system via fiber-optic cables to reduce the amount of EMI which is conducted to the control room. The output radiation is directed through a quartz window into the diagnostic area. Figure 3 shows the diagnostic that we have employed for frequency measurement: a "thin-film" filter and crystal detector.

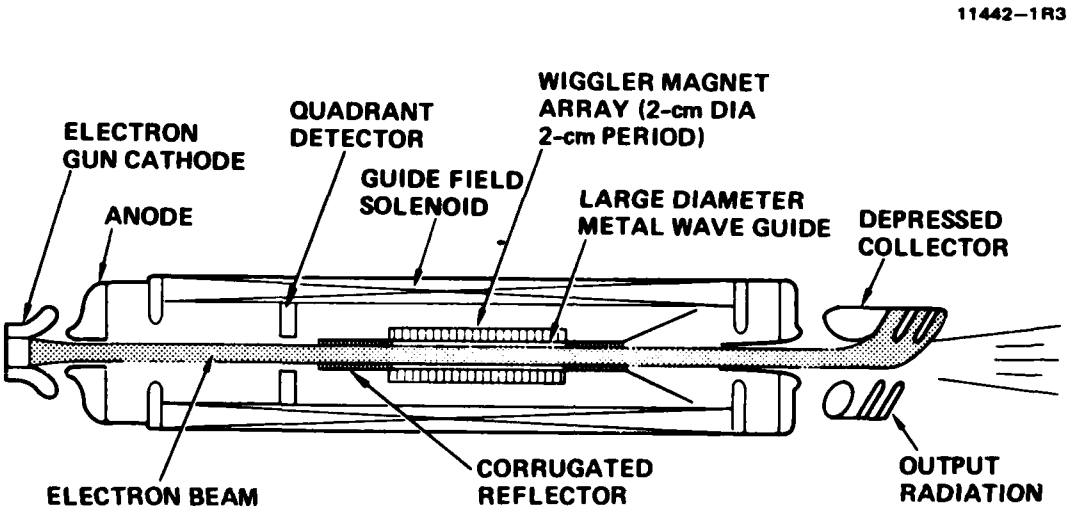

Figure 2. First stage test model.

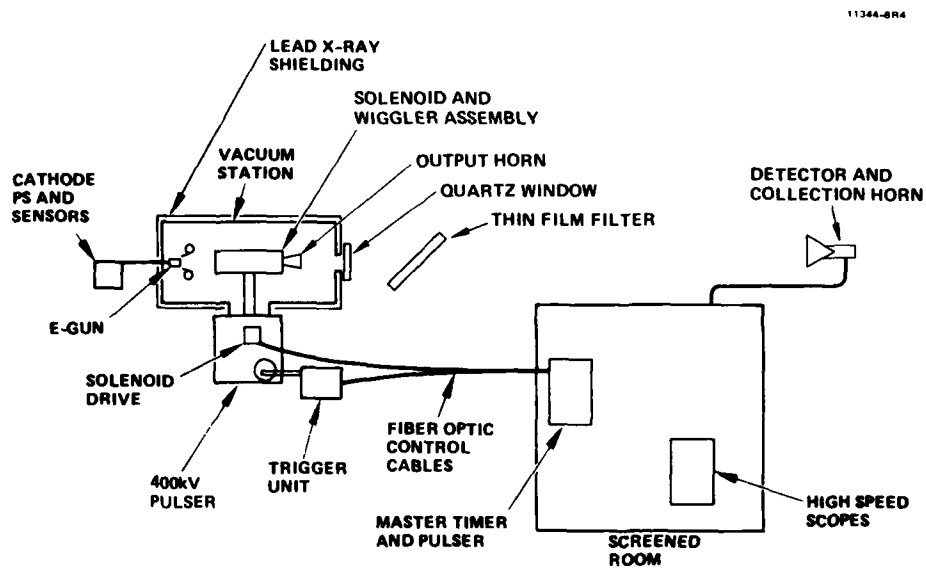

Figure 3. FEL experimental apparatus.

A. ELECTRON GUN

The E-gun has been described in a previous report[5]; however, we will briefly describe it here for continuity. The E-gun is a Pierce-geometry, non-gridded design which operates with the cathode at ground potential. It was designed to operate at 400 kV and 40 A, but has been operated at below 300 kV for the majority of these experiments. The electrode shapes were configured using the Herrmannsfeldt electron-trajectory code.[6] An iterative process was used to create electrode shapes which generate a laminar beam at the desired voltage and current. The output of this code is shown in Figure 4, while the embodiment of the code output is shown in Figure 5, along with individual components and the completed E-gun.

The cathode is 4 cm in diameter and produces a beam which is focused past the anode with a 1-cm diameter. The cathode, which is indirectly heated, is made of impregnated porous tungsten. The normal operating temperature of this cathode was expected to be approximately 1100°C; however, for most of these experiments operation in excess of 1200°C was necessary for appreciable current to be extracted. This is thought to have been due to impurities in the system which slightly poisoned the cathode and forced higher-temperature operation. The lower operating current may also have been due to possible contact of the field electrode to the cathode, causing the cathode edge to operate at a lower temperature than the bulk of the cathode. Near the end of these tests a cathode with an osmium coating was installed. This reduced the work function of the cathode and allowed operation at approximately 1000°C. Even with this improvement, however, the E-gun seldom operated at its full design perveance of 0.15×10^{-6} A-V$^{-3/2}$. The cathode typically operated at around 75% of the design perveance (e.g., 12.5-13 A at 230 kV).

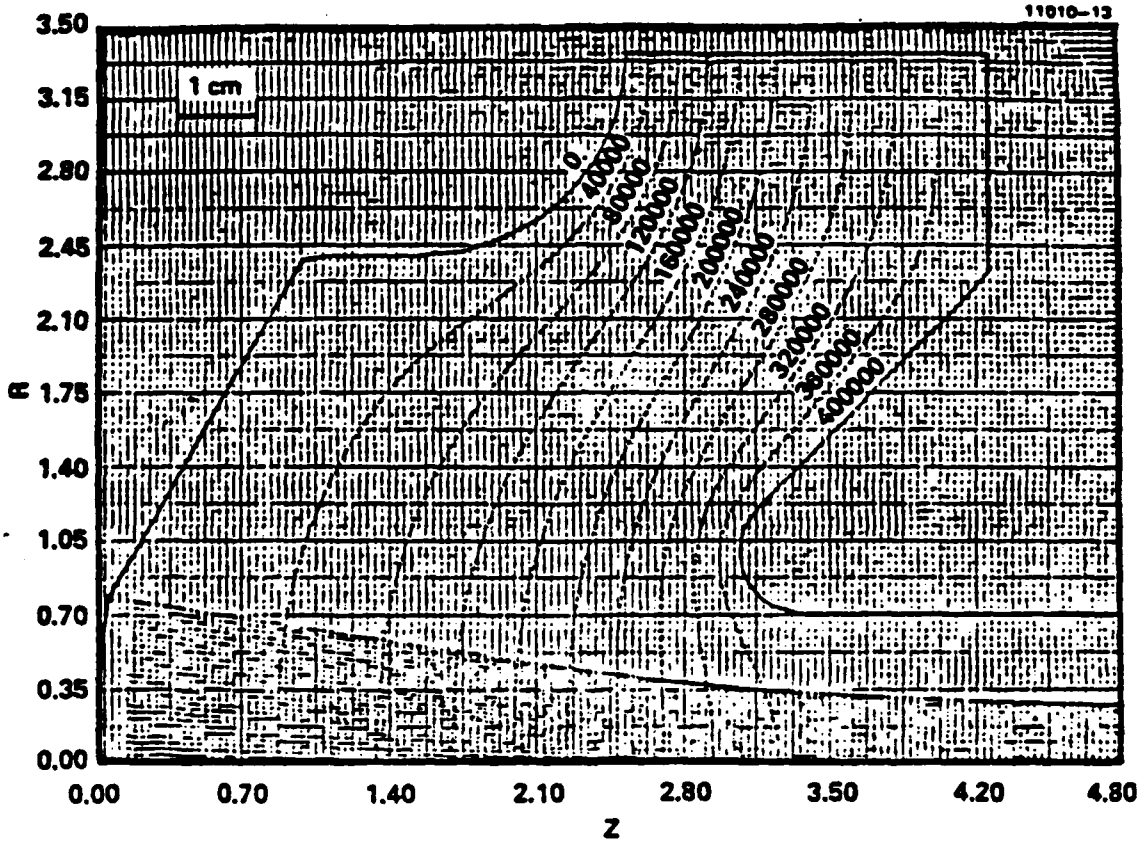

Figure 4. Typical computer plot of the electron trajectories and equipotential lines in the E-gun.

ELECTRON GUN

GUIDE FIELD

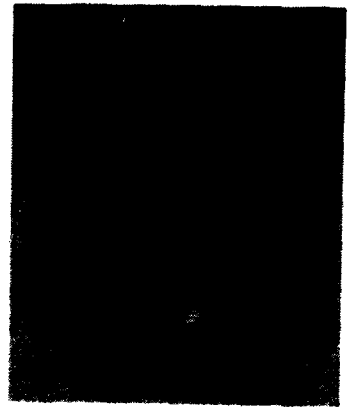

DEPRESSED COLLECTOR

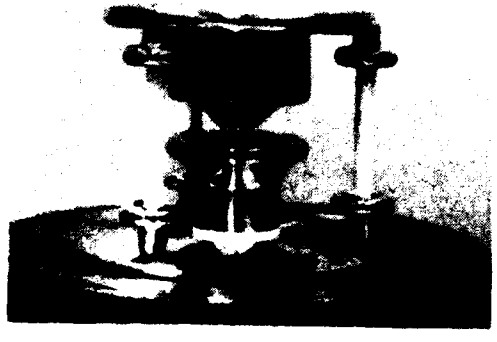

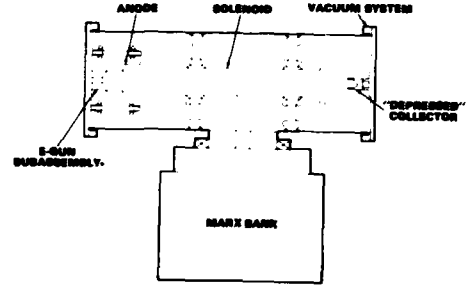

Figure 5. FEL components.

B. BEAM POSITION MONITOR

The E-beam position is monitored at the input of the solenoid by a quadrature detector, as shown in Figure 6. Four segments of an annular ring which are mounted on the periphery of the beam where each collects a small portion of the beam current as the beam passes. Each segment is connected to a light bulb. The relative brightness of each bulb gives a measure of the beam location.

Two different adjustment systems are provided to position the beam on axis. In one, a pair of steering coils is mounted on the outside of the vacuum chamber. The magnetic field produced by these coils acts on the beam until it enters the solenoid where the field is shielded by an iron-core-solenoid jacket. The orientation of the magnetic field, which is generated by these coils, is perpendicular to the electron velocity and, therefore, produces transverse motion. The orientation of the magnetic field can be adjusted by varying the current in each coil so that non-axial position can be compensated.

The other beam-adjustment system consists of a three-point-alignment jig on which the E-gun is mounted. The monitored position is altered, in this case, by changing the E-gun alignment with respect to the monitor axis. With these adjustments set properly, the beam enters the solenoid on axis. Since the quadrature detector is located at the input to the solenoid, the casing of which excludes the steering fields, it is assumed that the beam remains on axis into the wiggler region.

C. WIGGLER MAGNET

Two general types of wiggler-magnet configuration are appropriate for FEL operation. These configurations are

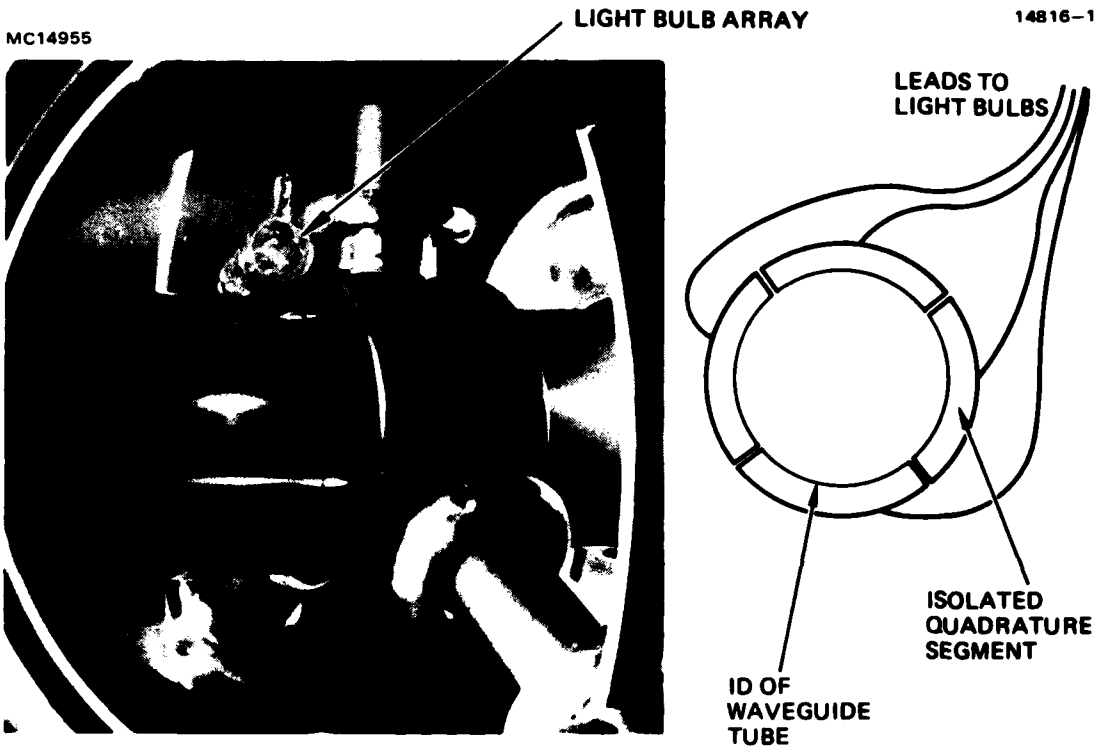

Figure 6. Beam monitor quadrature detector.

designated linear and helical, and correspond to the way the wiggler varies along the axis. The linear-wiggler magnetic field is plane polarized and oriented transverse to the E-beam motion. Its orientation alternates 180° each half period. The helical wiggler, on the other hand, is circularly polarized, with the magnetic-field orientation varying continuously in a corkscrew fashion along the axis. To date, we have tested only linear-wiggler-magnet configurations.

Under the class of "linear wiggler", we have designated a sub-class of wigglers according to the physical makeup of each design. The outline of these wigglers, linear and square, and a field-line plot of each is shown in Figure 7. The linear wiggler, shown in Figure 8, suffers from the defect that it is non-focusing. Even though the E-beam enters the wiggler on axis it will gradually drift to the side and finally hit the waveguide wall. The E-beam does not propagate completely through the resonator with the linear wiggler installed. As a result, FEL action with the linear wiggler was never observed.

The square wiggler design, shown in Figure 9, was suggested independently by workers at HRL and NRL[7]. It has been the most successful configuration we have attempted to date. The square-wiggler configuration consists of two linear wigglers oriented at right angles and, as a result of the improved symmetry, is self-focusing. An off-axis electron experiences a stronger magnetic field and more curvature of its trajectory the further it moves from the axis. The only exception occurs near the corners of the magnets, where some losses may occur. This has generally not proved to be a problem.

The wiggler magnet is a permanent-magnet design which eliminates the need to provide magnet power at high voltage (The wiggler, solenoid, and anode float at high voltage in the present system design.). The magnets are made of samarium-cobalt and have a residual magnetization of 9000 G. They were

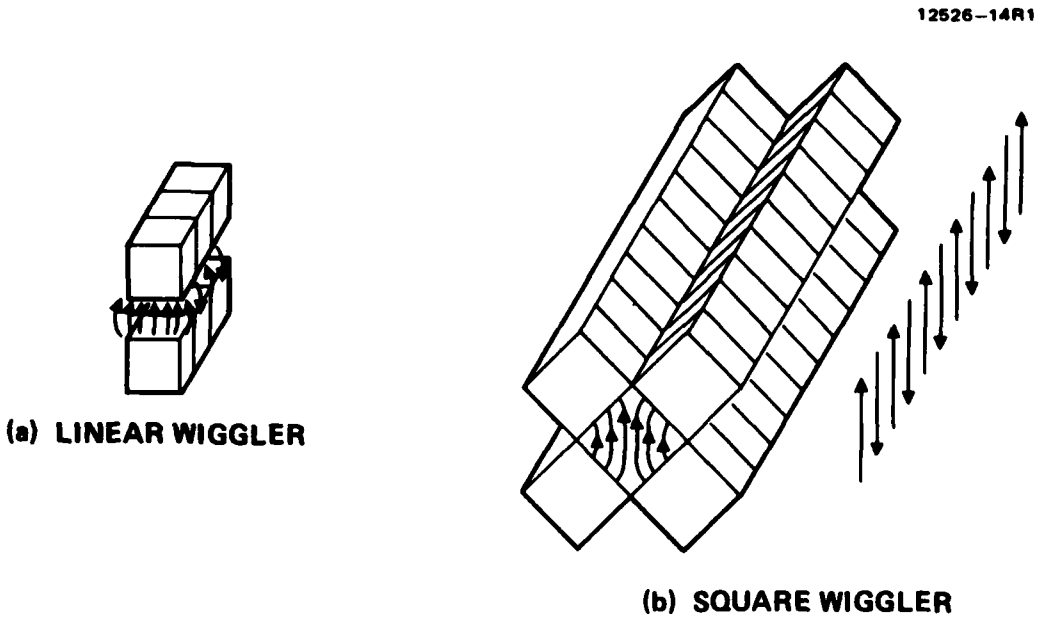

Figure 7. Wiggler magnet configurations.

M14322 12115-5

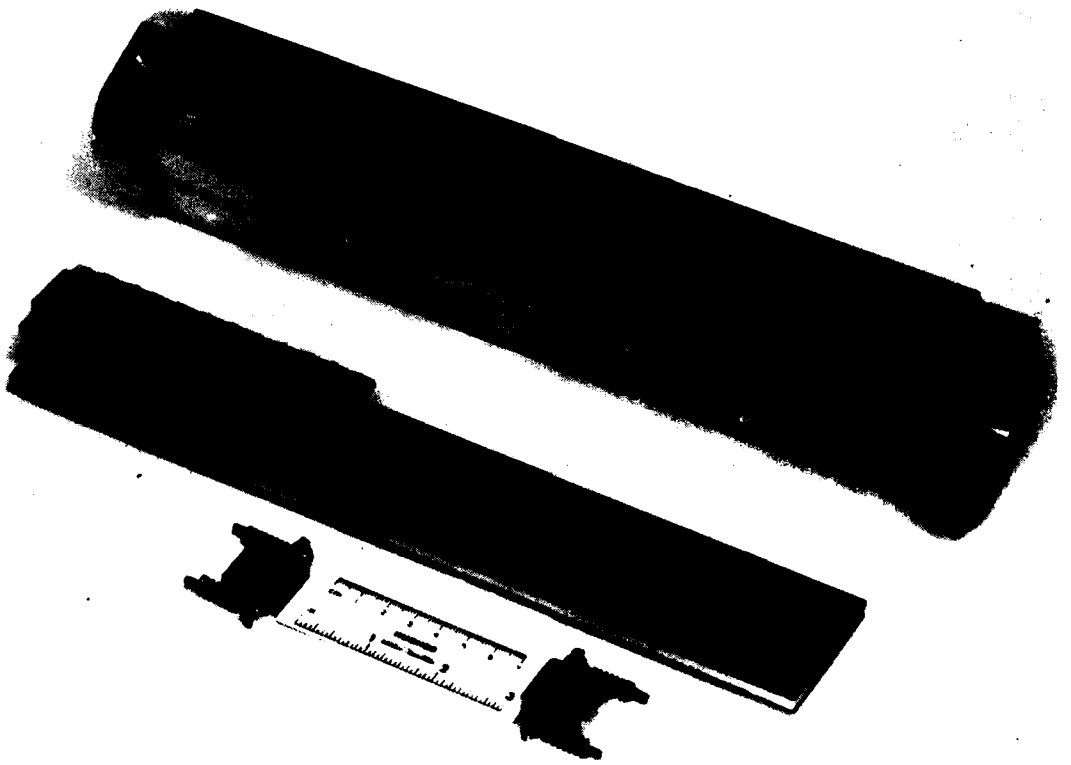

Figure 8. Linear wiggler structure (partial assembly).

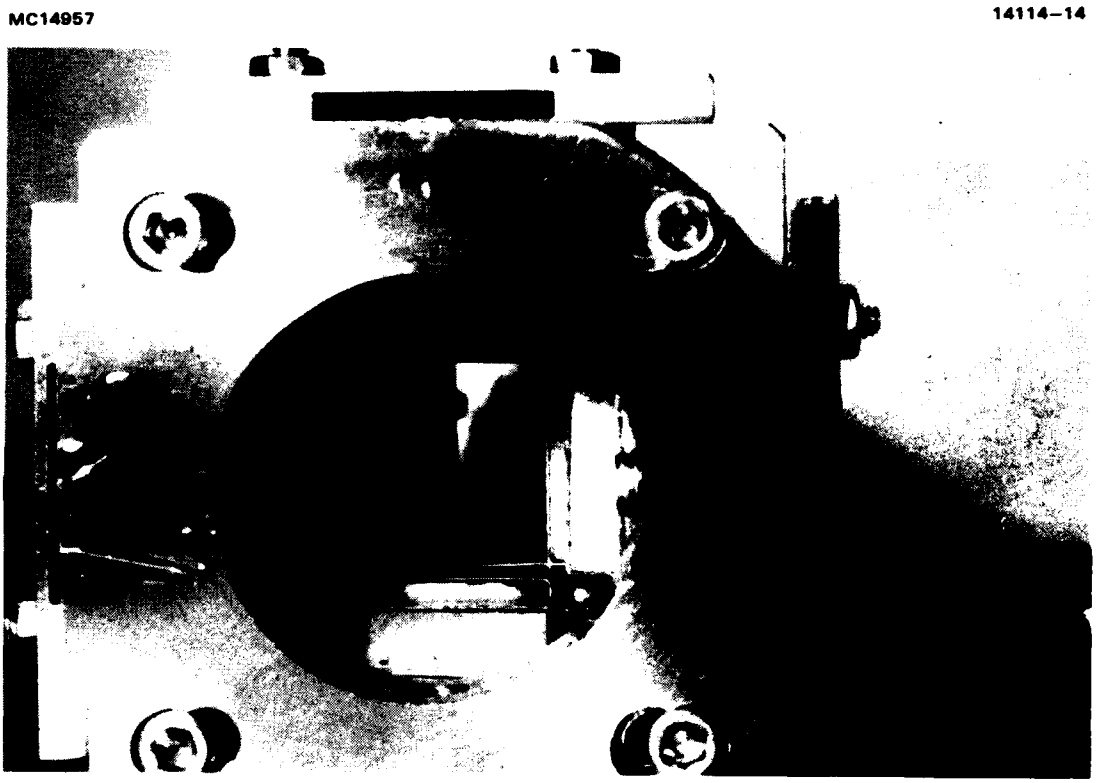

Figure 9. Square wiggler entrance.

manufactured by Colt Industries. The magnet assembly is 30 cm long with a 2-cm period. Each half period is composed of 4 magnets of dimension 2.5 cm x 2.5 cm x 1 cm. The on-axis field is polarized at approximately 37° to one side of the square with a peak field of 466 G. To maximize the on-axis field, one set of magnets is placed as close to the waveguide as possible, with the second set slightly further away; i.e., giving a slightly rectangular cross section and a polarization other than 45°.

A 4-magnet taper is provided at the entrance to the wiggler for "adiabatic" injection of the E-beam. A one-magnet adjustment is provided at the wiggler exit to compensate for the increase in magnetic field due to the final magnet. Each magnet has a two-point adjustment (for position and tilt) to account for magnet-to-magnet differences in magnetization. The magnet assembly is adjusted so that the magnitude of the field is uniform along the length of the magnet and so that the $\int B.dl$ is as close to 0 as is practical along the length of the wiggler for both the polarized wiggler field and for the transverse error field.

The apparatus for making magnetic-field measurements is shown in Figure 10. A Hall-probe-gauss meter is mounted on a motorized-drive screw and directed down the axis of the wiggler. The probe is constrained to stay on axis by having sliding contact between the probe mount and the waveguide tube. In this setup no provision is made for off-axis measurements-a situation which should be rectified on future experiments. A representative magnetic-field plot is presented in Figure 11. The wiggler field and the transverse field along the length of the wiggler are shown. One problem which came to light during this measurement is a rotation of the polarization orientation in the wiggler-entrance-tapered section. When viewing the field along either of the two axes (the standard technique for measuring the field), this feature was not apparent. The

MC14949 14816-2

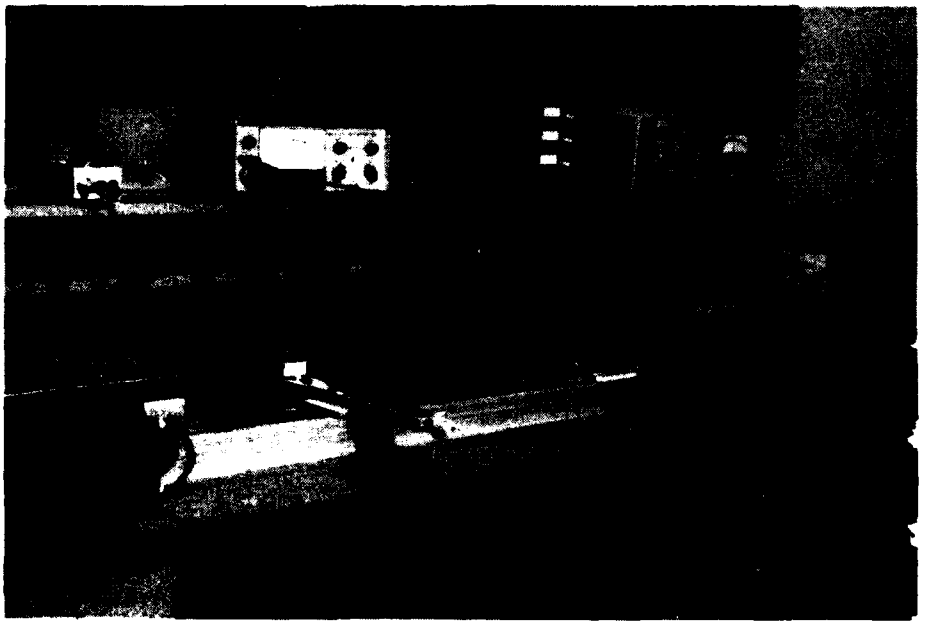

Figure 10. Magnetic field measurement apparatus.

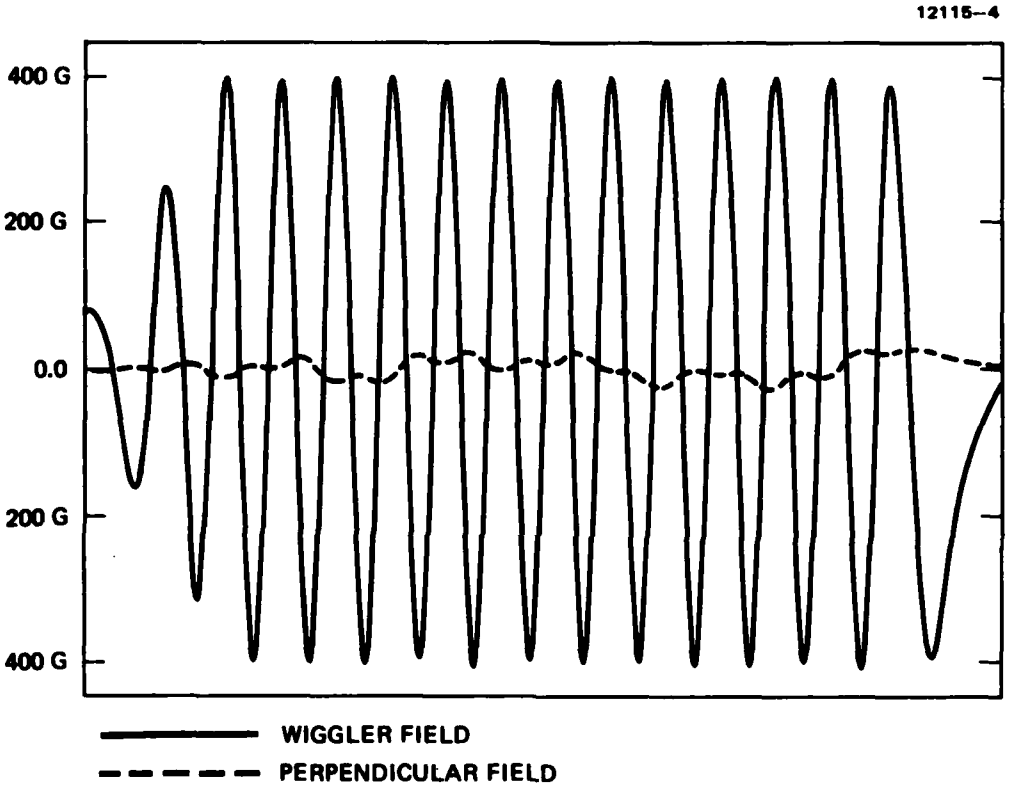

Figure 11. Plot of wiggler field and perpendicular field.

specific orientation of each magnet set had to be viewed individually in order to see this effect. Care must be taken to assure that the entrance orientation matches that of the main wiggler.

D. RESONATOR

The present brassboard FEL is a relatively low-gain device; therefore, for a reasonable length of the wiggler, a high-Q resonator must be utilized to assure successful operation. The chosen resonator consists of a smooth, over-moded, waveguide tube with reflectors at each end. Three different resonator configurations have been tested during the course of the present program. These configurations include a quasi-optical concentric resonator, a screen resonator and a distributed-Bragg-reflector resonator.

The only successful resonator used distributed-Bragg reflectors on either end of a cylindrical waveguide, as shown in Figure 12. The reflectors, which will be described later, provided the high reflectivity needed for a high-Q resonator and, at the same time, presented a large aperture to allow passage of the E-beam. The maximum value of Q measured with a resonator using distributed-Bragg reflectors was 18000. This value of Q corresponds to a round trip loss of about 2%.

The other two resonators, concentric and screen, are shown in Figures 13 and 14, respectively. The concentric resonator, which has been used successfully in gas waveguide lasers,[8] is composed of 2 spherical mirrors located so that the mirror focal point is near the waveguide entrance. The mirrors have axial apertures to allow passage of the E-beam. The area of these apertures represents a cavity loss of about 10%. The maximum Q measured with this resonator is 4100, which corresponds to a loss of 16% per round trip. The increase in loss is believed to be due to mode conversion at the waveguide

MC14945 14114-12

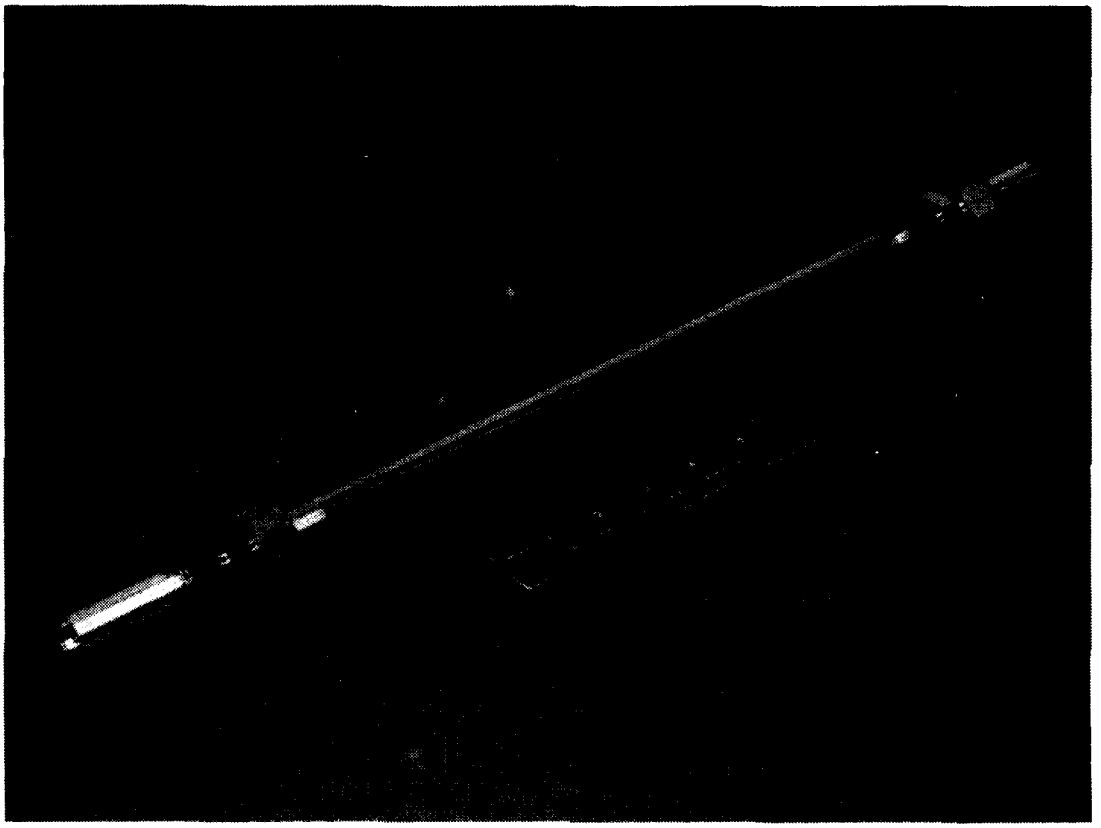

Figure 12. High-Q cavity.

MC14367 13572-40

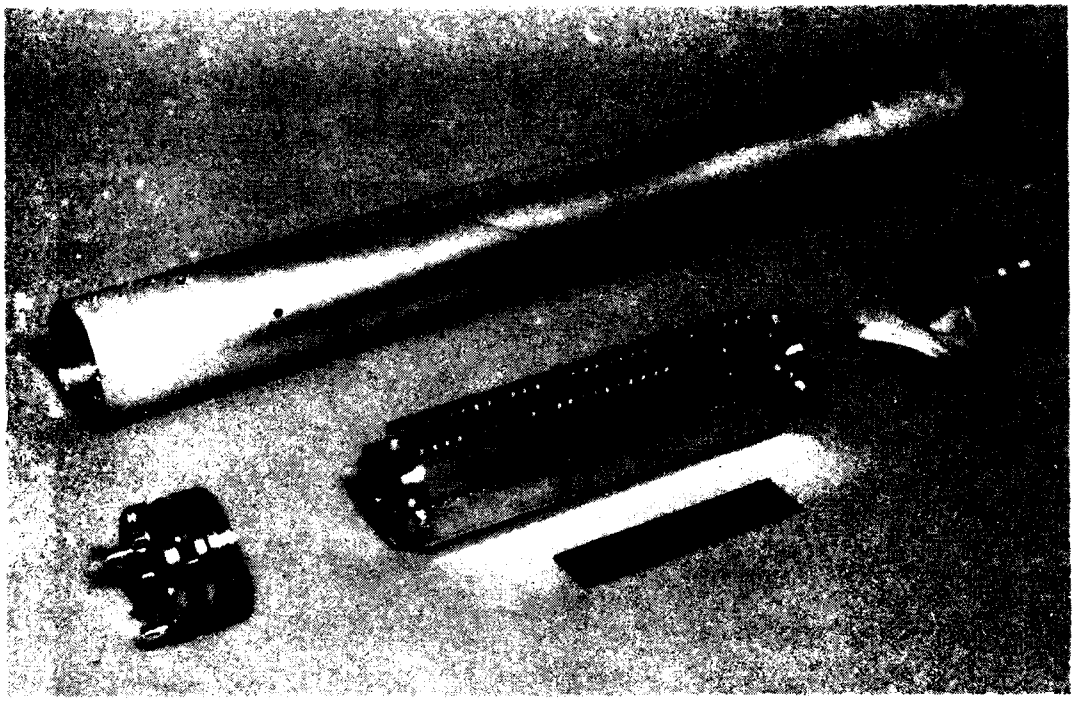

Figure 13. Concentric resonator assembly.

M16433 14816-3

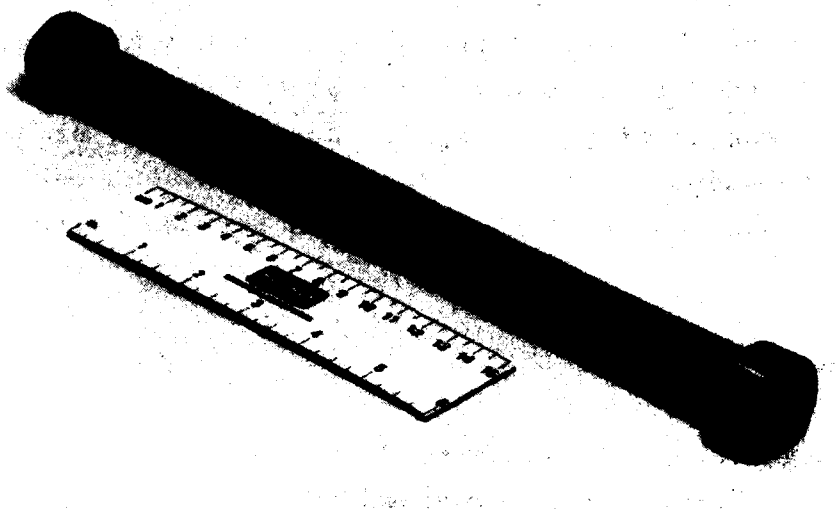

Figure 14. Screen resonator.

exit. Attempts were made to compensate for mode conversion by adding horns to the system and by reducing the size of the mirror aperture. Improvements in the Q were seen, but they were not sufficient to allow forward wave operation of the FEL. The screen resonator exhibits a high Q; however, it suffers from interception of the E-beam by the screen and the subsequent formation of an ablation plasma during the pulse. Interception of the beam by the screen reduces the available current and, therefore, the gain is also reduced. At the same time, the presence of plasma spoils the cavity Q, driving the system below the threshold for lasing action. Other than occasional noise bursts, FEL action was not seen with this resonator.

E. POWER SUPPLY

The E-gun operates at up to 300 kV and 15 A for these experiments. The power is provided by an air-core, pulse transformer, shown in Figure 15, driven by the tuned pulse-forming network shown in Figure 16. Earlier work was done with a Marx-bank generator; however, the pulse flatness was not sufficient. The circuit diagram of the power supply is shown in Figure 17. This 5-section, pulse-forming network produces a variety of pulse shapes, depending on the inductance of each section. Flat-topped pulses of up to 30 μs in length have been generated. The length of the pulse depends on the circuit inductance and on the specific transformer design. The high-voltage switch is fired via a fiber-optic link, thereby reducing conducted EMI to the control room.

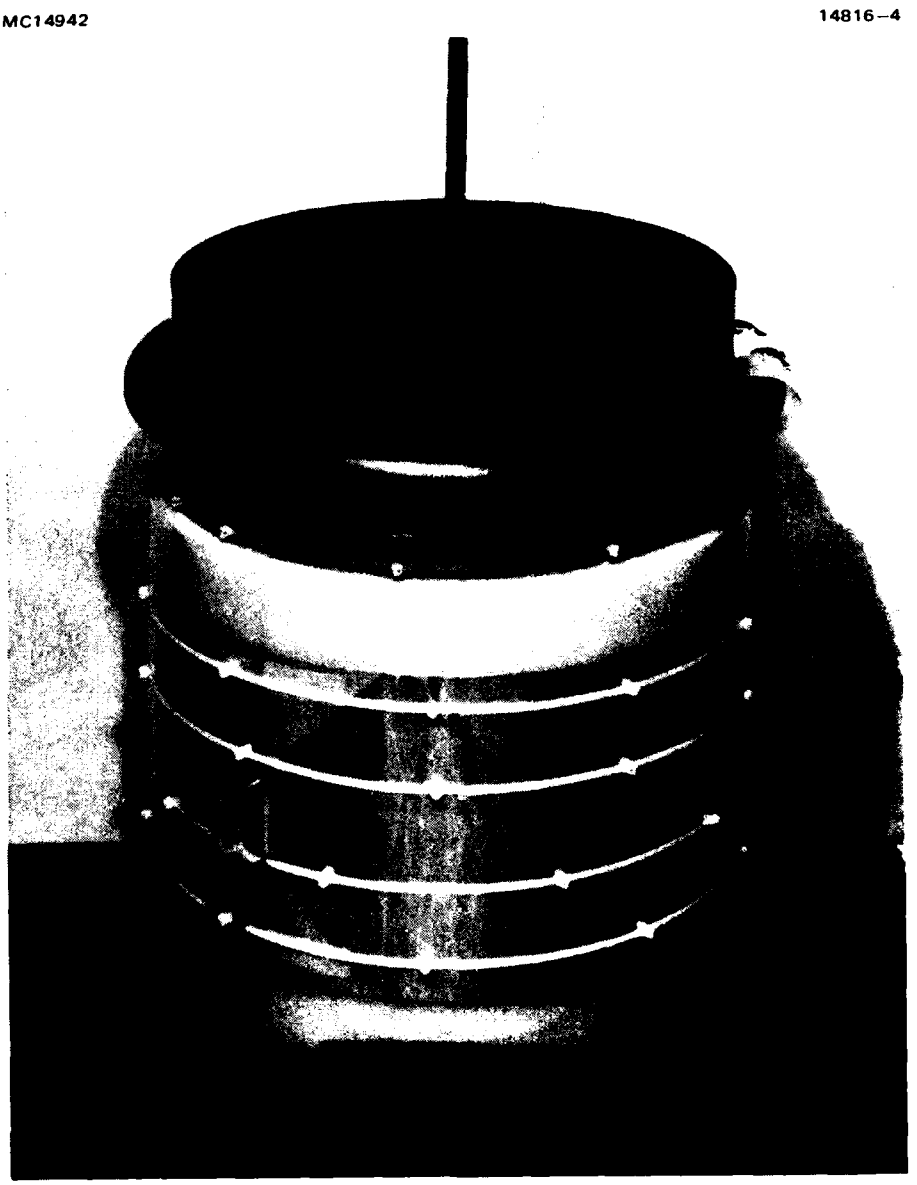

Figure 15. Air-core pulse transformer.

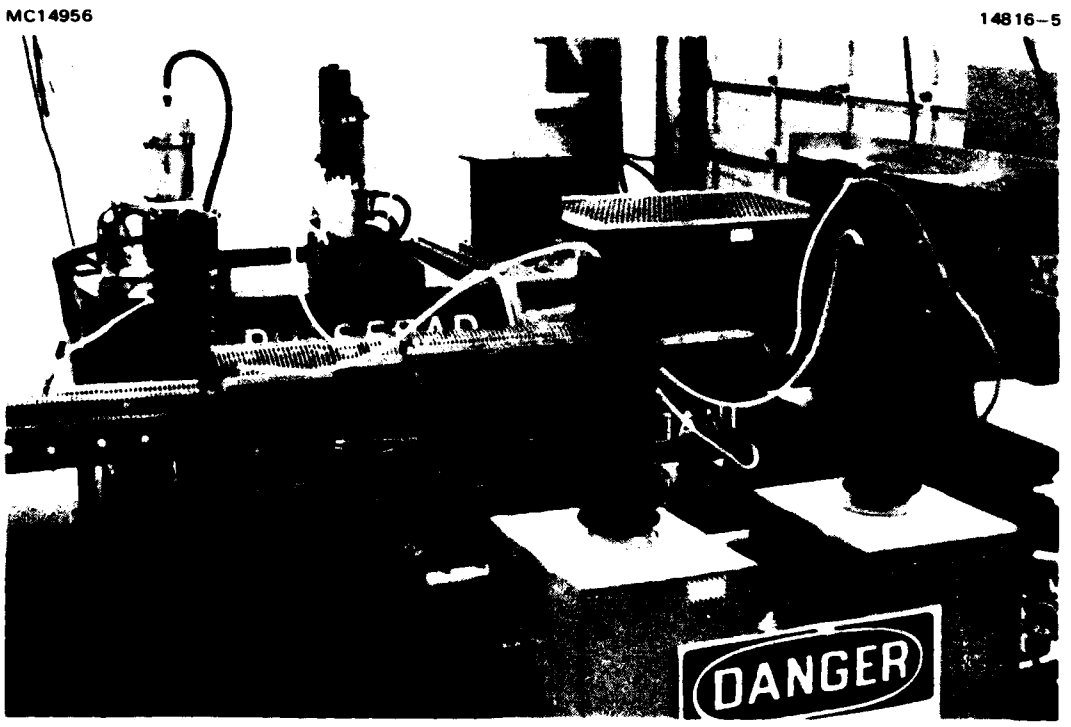

Figure 16. Tuned pulse transformer network.

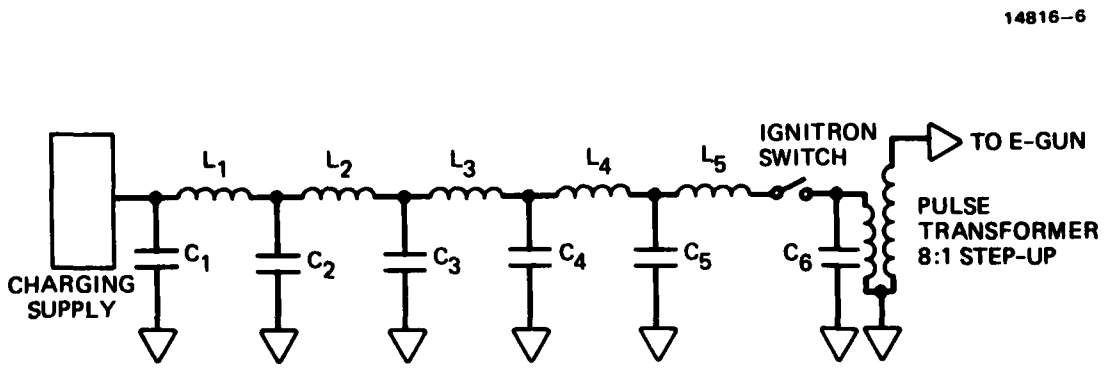

Figure 17. Power supply circuit design.

F. DIAGNOSTICS

FEL radiation is directed through a quartz window into the diagnostic area. Since the FEL output aperture is some 70 cm from the small (10-cm-dia) output window, only 10% of the beam gets into the diagnostic area. Beam expansion within the vacuum chamber, and the fact that the device operates with a single pulse of short time duration, means that the per-pulse energy density in the diagnostic area is small except (possibly) near the output window. Samples of the radiation are collected with a crystal detector and waveguide horn.

Power estimates are made by scanning the detector horizontally to obtain an output-radiation pattern. The area ratio of the mode pattern to that of the collection horn, the collection efficiency of the horn, the output aperture attenuation and crystal detector power calibration are taken into account to get a total output power estimate. The total system attenuation generally is 10^{-5} to 10^{-6}, depending on detector location.

The frequency measurements were made with a "thin-film", interference filter. This filter is composed of alternate, quarter-wave thicknesses of plexiglass and air. The theoretical-response curve is shown, along with experimental data points, in Figure 18. The frequency is determined by measuring transmission through the filter which is placed at various angles with respect to the output window and comparing the results to predicted curves.

Polarization of the radiation is determined by rotating the collection horn about the axis and comparing the intensity verses angle data. The horn is designed to collect TE_{11}-mode radiation and as such is an excellent polarization detector. However, errors in polarization measurements can arise due to reflections from window edges and due to obstructions located between the FEL and detector.

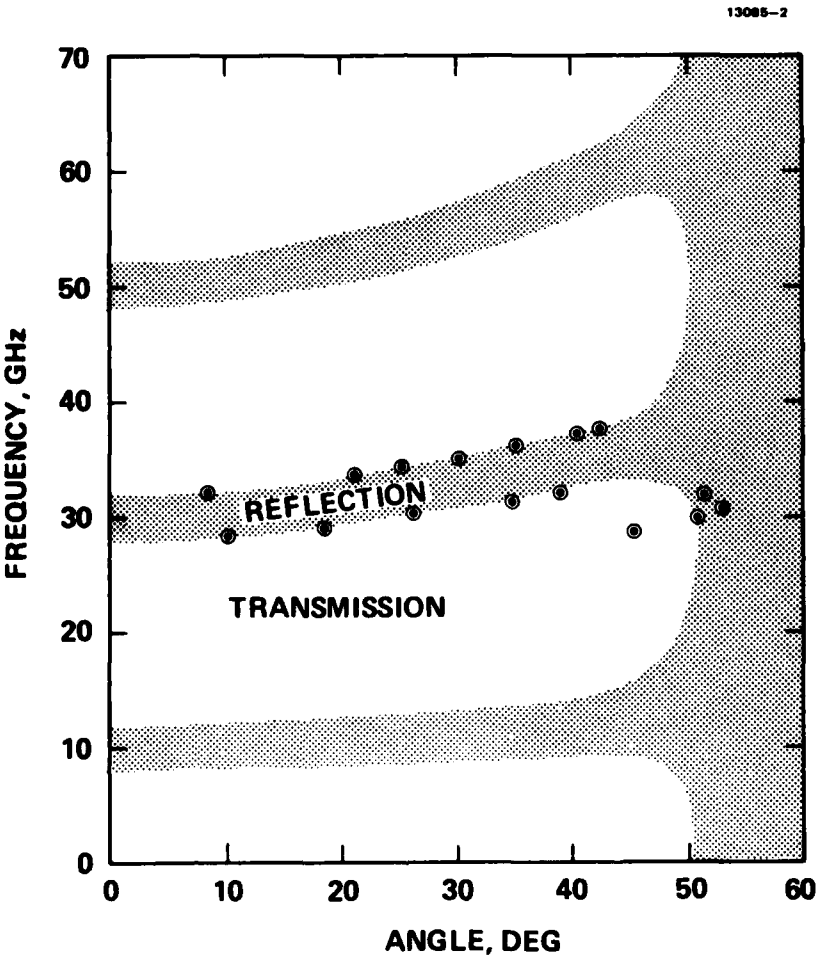

Figure 18. "Thin-film" filter response. The data represent 50% transmission points.

SECTION 3

THEORETICAL BACKGROUND

The emission from a FEL operating in a waveguide is given by the coupling of the FEL interaction equation with that of the electromagnetic waveguide mode. The free space FEL interaction is described by the equation,

$$\omega = \beta_{||} c(k_{||} + k_w). \tag{1}$$

The electromagnetic waveguide mode is described by the equation,

$$\omega^2 = c^2 k_{||}^2 + \omega_c^2. \tag{2}$$

In these equations ω and $k_{||}$ represent the FEL radiation frequency and axial wavenumber, respectively; ω_c is the waveguide cutoff frequency; k_w is the wiggler wavenumber; and $\beta_{||} = v_{||} / c$ is the beam axial-velocity characteristic. These equations presume that the plasma frequency of the electron beam is negligible (i.e., $\omega_p << \omega_c$) and that the magnitude of the wiggler field remains constant. The strength of the wiggler magnetic field, however, increases with distance from the axis. The E-beam itself is of finite size and electron trajectories are not strictly on the axis; a shift in the frequency of operation is a consequence. For our magnet

configuration, the frequency shift due to the E-beam experiencing different magnetic field values is given by

$$\frac{\Delta\omega}{\omega} = \left(\frac{3}{4}\right)\left(\frac{e}{m}\right)^2 \frac{(1+\beta)}{k^2 v_{zo}^2}\left(B_{xo}^2\cosh^2(kx) + B_{yo}^2\cosh^2(ky)\right) . \quad (3)$$

The frequency is also shifted by extraction of energy from the E-beam during lasing action because $\beta_{||}$ is directly affected. The solution to Equations (1) and (2) with the frequency shift factored in is shown graphically in Figure 19. Here, the upper portion of the curve and the portion continuing around the knee of the curve to about 180 kV is the forward-wave branch and the remainder of the lower portion is the backward-wave branch. Since the backward wave operates at the cutoff of the waveguide, no additional resonant structure is required (i.e., the Q of the waveguide alone approaches 10,000 at cutoff). For the forward wave, the frequency-shift effects manifest themselves as a shift in operating voltage for a given frequency. When a high-Q resonator is present within the system, the forward-wave is constrained to operate at a given, distinct frequency or set of frequencies. Therefore, the FEL operates at the frequency of the high-Q resonator mode. Shifts in the operating conditions are reflected in shifts in the operating voltage of the FEL.

Our FEL operates on the border between the Compton and Raman regimes, since the longitudinal wavenumber ($k_{||}$) is

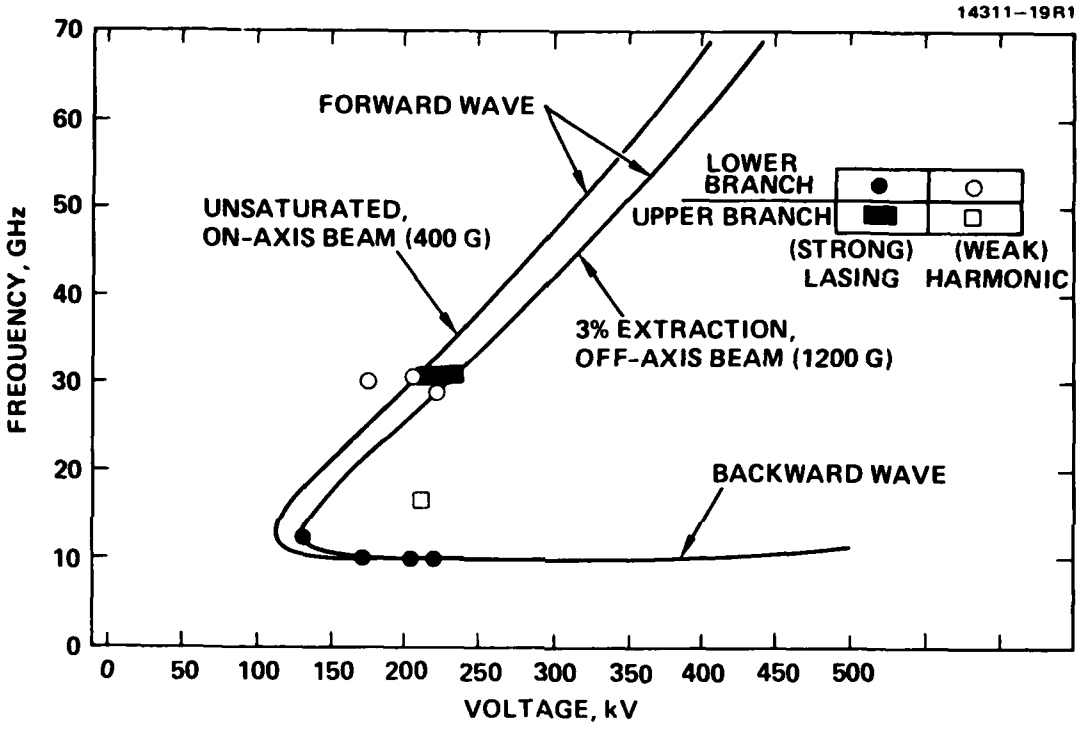

Figure 19. Correspondence of FEL data with dispersion theory.

approximately equal to the Debye wavenumber.[9] The gain is, therefore, given by the equation

$$G = \frac{\pi}{4}\left(P\ \frac{\gamma\omega_p^2}{w_s^2}\right)(\pi/k_w)^{-2}\frac{k_s}{\gamma^2}L^3 \quad , \qquad (4)$$

where $P = e^2B_0^2F/m_e^2k_0^2c^4$, ω_p is the plasma frequency, ω_s is the signal frequency, k_s is the signal wavenumber, B_0 is the wiggler field value, k_0 is the wiggler wavenumber and F is the E-beam fill factor. The gain has been plotted for a range of operating voltages. The results are shown in Figure 20. The gain plotted here is between 24 and 32% for the forward wave, and between 16 and 10% for the backward wave over the voltage range of interest. The forward wave gain should dominate over the backward wave; however, the resonator Q has a significant role in determining which mode of operation occurs.

The backward wave operates at the cutoff frequency of the waveguide and the forward wave operates at the frequency of the resonator mode. If the Q of the resonator for the backward wave is significantly higher than that for the forward wave the backward wave will dominate over the forward wave.

The Q of the resonator for the backward wave can be estimated by the Q of a right-circular cylinder, shown in Figure 21. At 10 GHz (the waveguide cutoff frequency) the Q is 10,000. Therefore, the Q of the resonator for the forward wave must not be significantly lower than 10,000 or else the backward wave will dominate. Therefore, from the outset our concentric resonator (with a Q = 4100) had only a marginal chance of success. In all cases, plasma formation and surface irregularities can significantly lower the value of Q and may cause the backward wave to dominate.

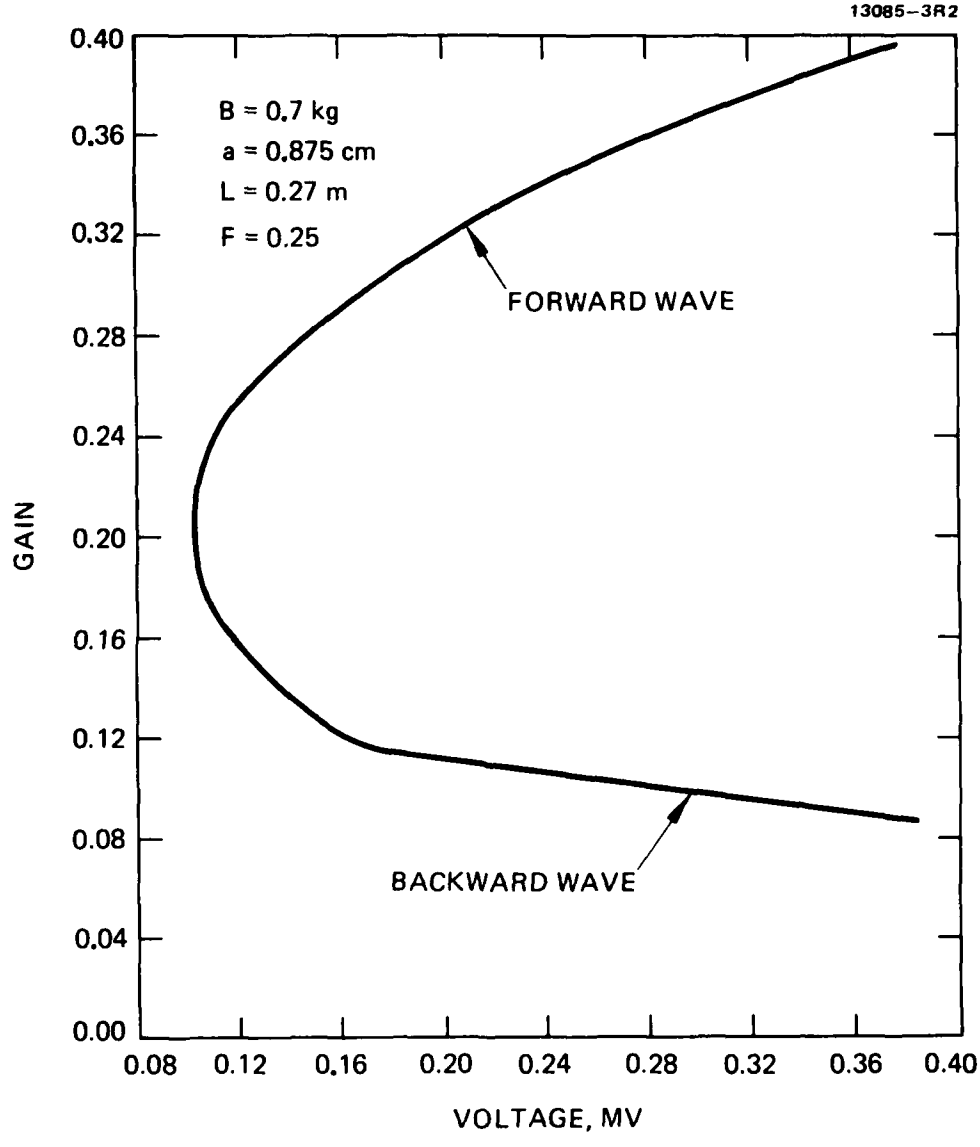

Figure 20. Predicted FEL gain characteristics.

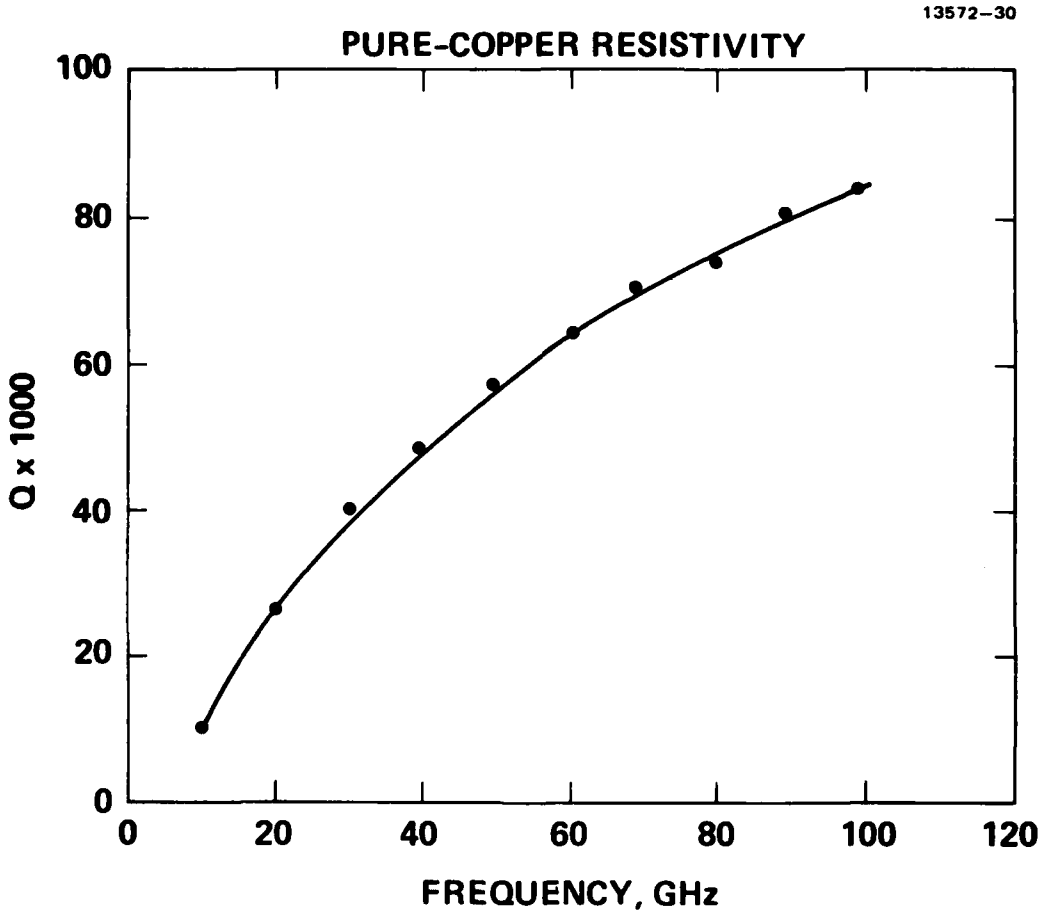

Figure 21. Q of a right-circular cylinder with end plates as a function of frequency.

SECTION 4

RESULTS

We collected and analyzed the output radiation of the Hughes FEL device when operating in both the forward and backward modes and determined the frequency for operation in both modes. We also determined the total output power and the polarization of the output radiation. The timing of the onset of radiation was used to estimate the system gain.

A. RADIATION FREQUENCY MEASUREMENTS

The FEL output radiation is collected with crystal detectors and collection horns in several bands. The frequency of this radiation is determined using the "thin-film" technique described earlier. When the Q of the cavity is such that the forward wave dominates, the frequency is determined by comparing the transmitted signal as a function of filter angle with experimentally determined calibration curves. An example is shown in Figure 22. The measured frequency is 30.7±.75 GHz. The frequency uncertainty is due to the limit of the resolution of the filter, which is determined by the number of layers in the filter and the radiation diffraction angle. Since the width of a resonant mode measured on the bench with a frequency meter and a klystron source is much narrower than the resolution of the measurement (i.e., ~2MHz), it is possible that several modes (lines) are present simultaneously. The frequency of the backward wave was determined to be 10 GHz using theoretically defined calibration curves, since an X-band source was not available for filter calibration.

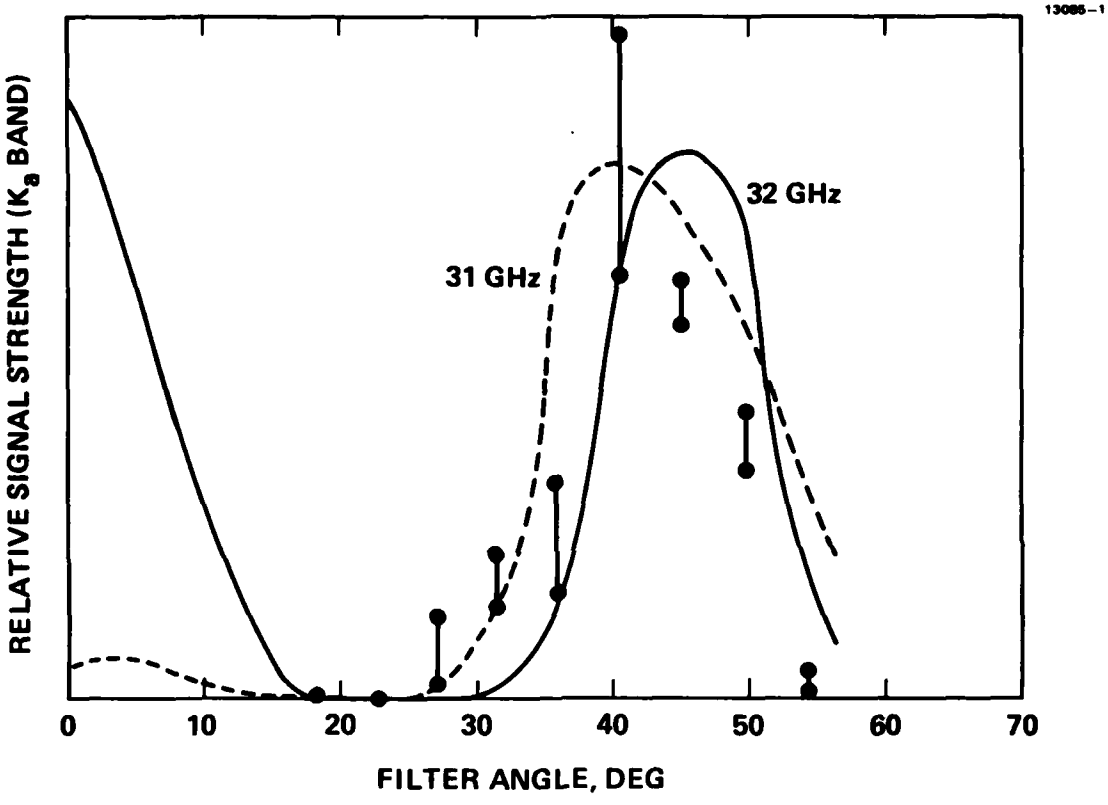

Figure 22. Identification of 31-GHz line at 181 kV. The dashed and solid curves are the closest matching calibration curves obtained at 31 and 32 GHz, respectively.

B. OUTPUT POWER DETERMINATION

The output power in the forward wave is measured by placing the detector at 13 m from the output window (to keep the detector from saturating) and working back through various diffraction angles and attenuations to reach an estimated output power. Based on the resonator parameters, losses about equal in magnitude to the output power are assumed to take place within the high-Q resonator. Therefore, the power generated by the FEL is twice the measured emitted power. The forward-wave power generated by the FEL using the distributed-Bragg-reflector resonator is then 120 kW. This power is generated at 224 kV and 13 A; therefore, the efficiency is 4.1%, which agrees well with the theoretically expected value of 3.7%, based on the linewidth of the laser.

For the backward wave, it is not as straightforward to estimate the output power. This is due to the fact that the waveguide is operating at cutoff and in the presence, in some tests, of other apertures (mirror holes) with cutoff frequencies above that of the backward wave. We estimate the power in the backward wave to be between 10 and 100 kW.

C. GAIN OF THE BACKWARD-WAVE BRANCH

The signal strength has been monitored in several frequency bands as a function of voltage and polarization. In Figure 23, we show an example of lasing action as measured with an X-band detector at a beam voltage of 214 kV. Similar signals, lasting for durations of up to 12 μs, are observed to correspond to resonances near 10 GHz; these are assumed to represent FEL action on the lower (or "backward-wave") branch of the FEL dispersion curve of Figure 20. These resonances are sensitive to voltage, guide-field intensity and beam alignment; they often exhibit line structures as narrow as 1 kV in

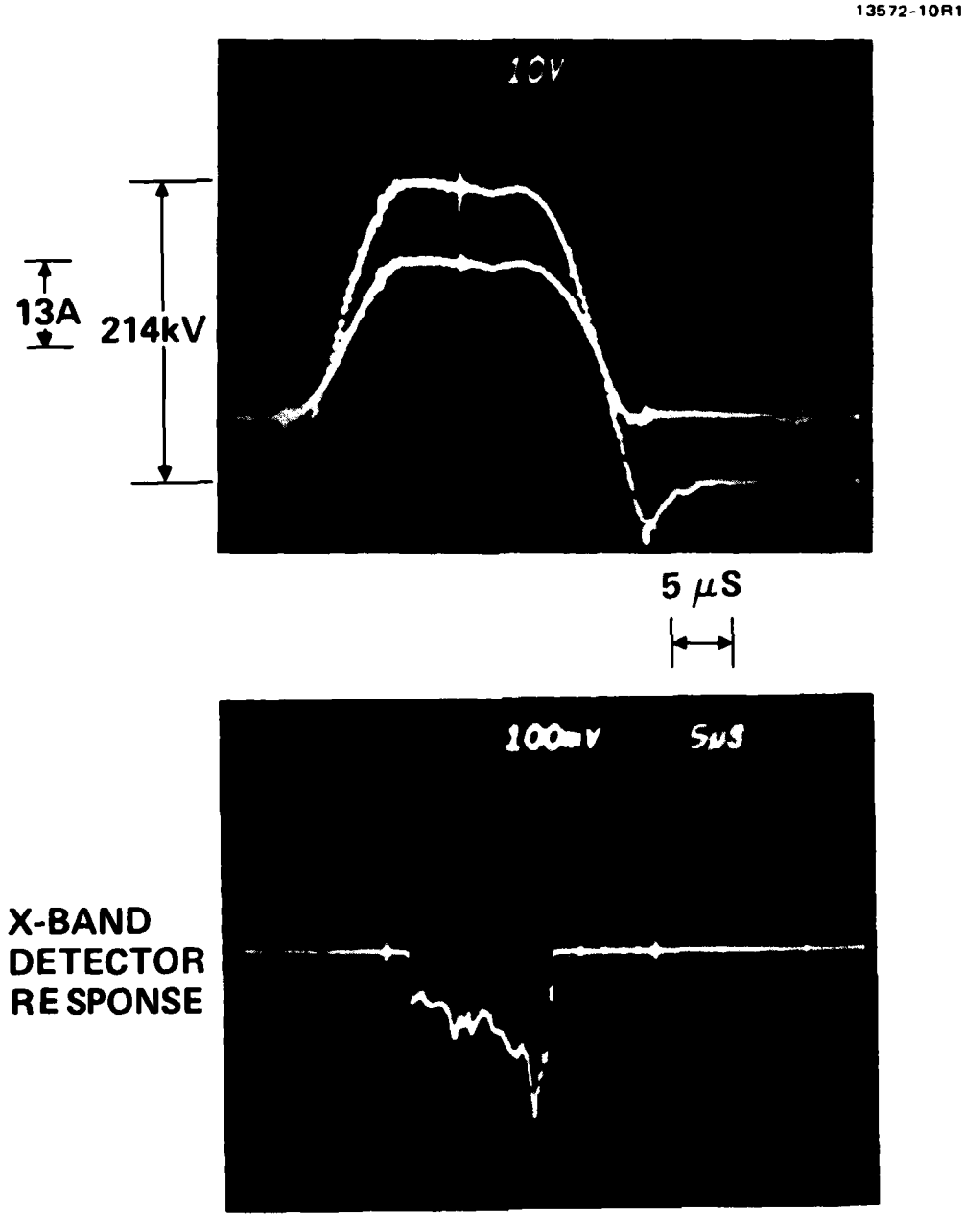

Figure 23. X-band response at 214 kV.

voltage. The net gain is estimated by varying the voltage and observing the timing of the first appearance of the identifiable lines during both the rising and falling legs of the voltage pulse. Based on the apparent 1.5 to 2-μs dwell times, during which the signal grows out of the noise, and upon the cavity parameters, the net gain has been estimated to be 2.5 to 3.3%. After correcting for cavity losses, the actual laser gain in the backward mode is estimated to be 5 to 6% per single pass.

D. GAIN OF THE FORWARD-WAVE BRANCH

The behavior near the upper (or forward-wave) branch of the dispersion curve is similar to the lower branch, although lasing action is confined to a narrower range in voltage space due to the vastly different slopes of the curves. Figure 24 shows the response of a remotely located Ka-band detector. Once the voltage reaches the resonant voltage, the signal requires approximately 2 μs to grow out of the noise; this dwell time corresponds to a net gain of 2.5% per pass and a laser gain of 4.6% (using the measured cavity Q of over 10,000 with an equivalent cavity-loss factor of 0.02 per double pass). Lasing is observed near 31 GHz over a voltage range starting at about 209 kV and extending to 235 kV, as shown in Figure 25. Since the frequency is determined by the cavity, the signal strength is a measure of the variation of saturated gain with voltage. The lower limit, at 209 kV, corresponds closely to the theoretical value for the expected voltage in the unsaturated case; the upper limit matches the expected voltage at saturation.

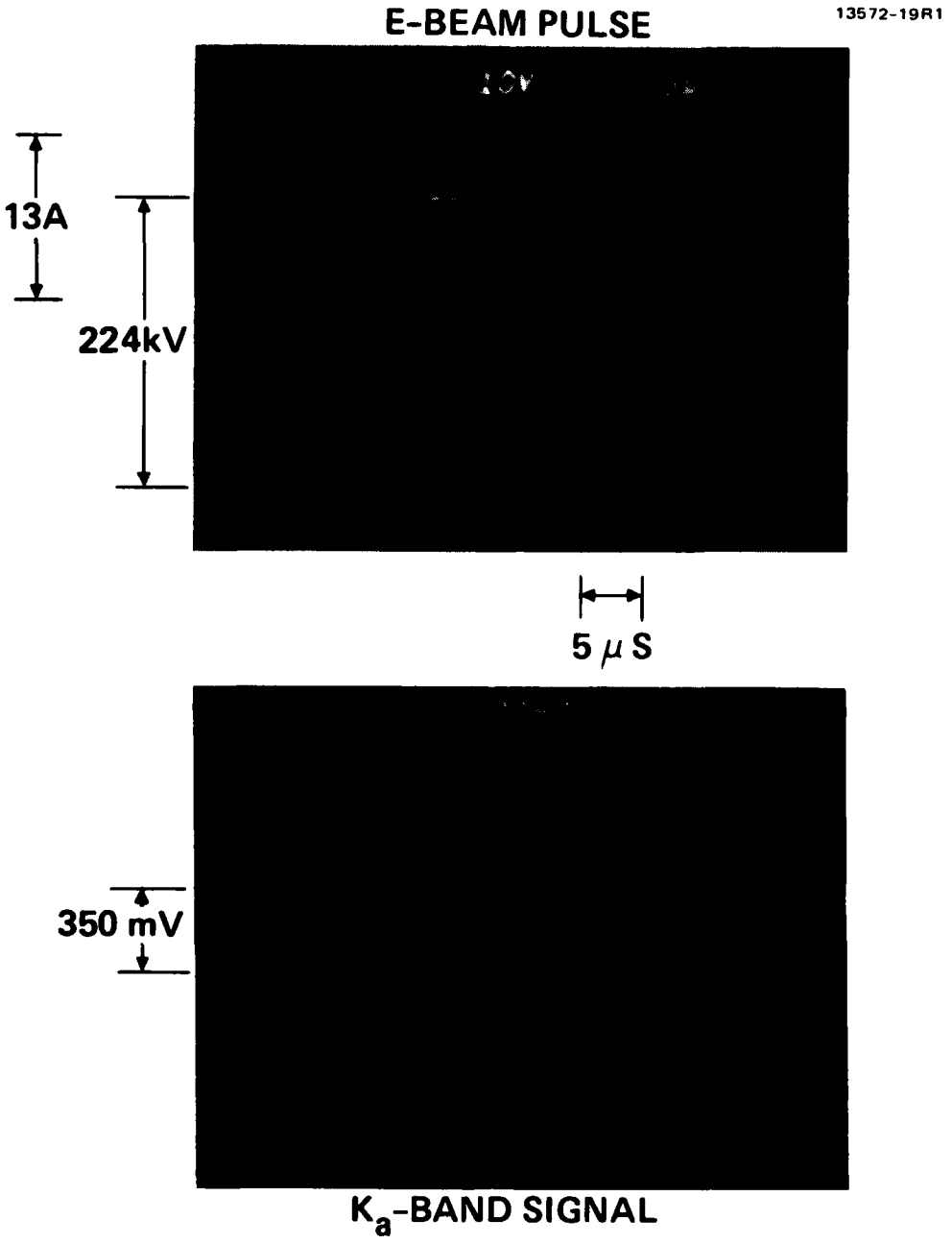

Figure 24. Example of K_a-band signal at 224 kV.

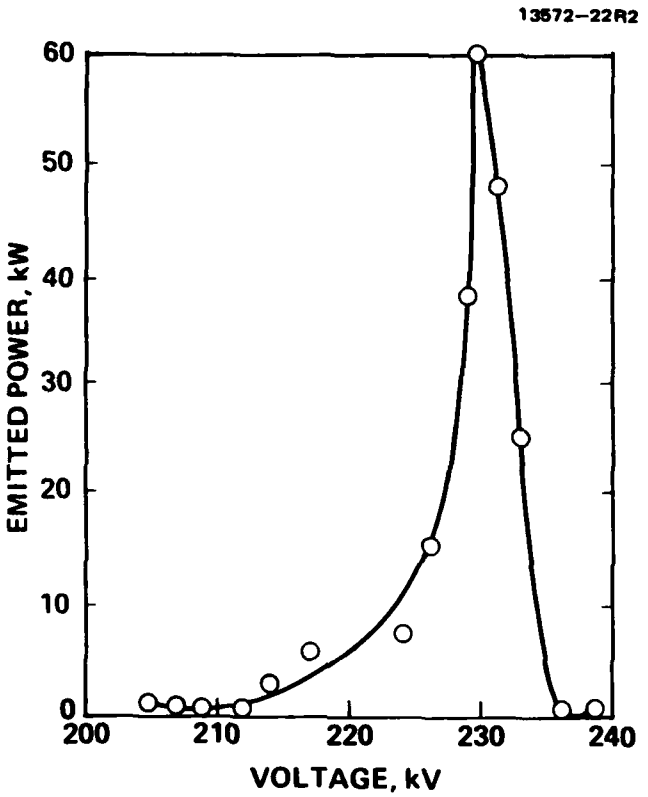

Figure 25. Forward-wave power vs. voltage with distributed-Bragg-reflector resonator.

E. LINEWIDTH

As the power in the signal wave builds (to 120 kW of extracted power), the resonance voltage is pulled to higher values to compensate for loss of energy by the electrons. Eventually the saturated power of the FEL is reached and the gain falls off rapidly with voltage. The width (FWHM) of the line (in voltage space) is measured to be 1.7%. By comparison, the effective wiggler linewidth (1/2N, where <N> = 13.5) is about 3.7%, or, transformed into linewidth in voltage space, is given by $\Delta V/V = (\gamma+1)/2\gamma \cdot 1/2N = 3.1\%$. When operating near the threshold gain, as was the case in these experiments, the measured linewidth would be expected to be somewhat narrower, which would put the experimental results in good agreement with the model.

The direct frequency measurements show a center frequency of 30.7 GHz and a linewidth of 1.5 GHz (or 4.8%); this linewidth is at the limit of the resolution of the instrument. The high-Q modes of the cavity are at 30.0, 30.3, and 30.7 GHz, which suggests that two or three of the modes, each about 2-MHz wide, have actually lased.

F. HARMONIC GENERATION

We have previously reported[4] observing the generation of third-harmonic output which is correlated to lasing action on the lower branch of the FEL dispersion curve. When the resonator is arranged for a high-Q resonance in the forward branch (to be excited at 31 GHz), the 10-GHz lower branch does not lase. Instead, a 16-Hz subharmonic is emitted at lower power. As shown in the example of Figure 26, the amplitudes of the harmonic and subharmonics are always considerably smaller than the primary lasing signals. Changing the cavity geometry or the beam alignment generally results in significant variation in the intensity of the harmonics with voltage.

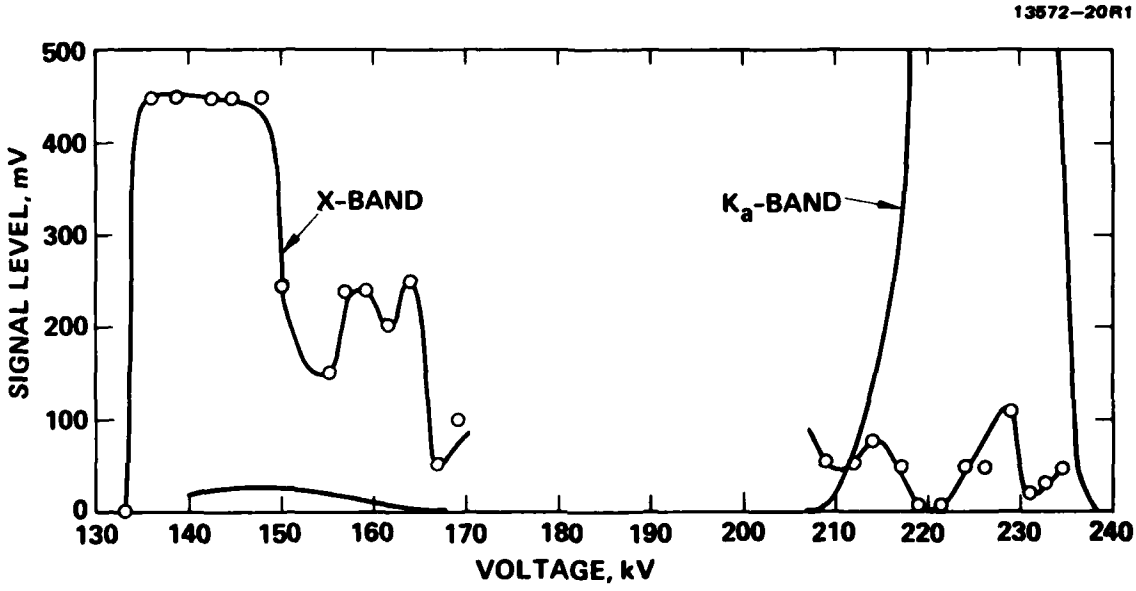

Figure 26. FEL output as a function of voltage in X- and K_a-bands. Curves with data points are X-band and smooth curves are K_a-band signals.

G. POLARIZATION

The polarization data shown in Figure 27 indicate that lasing action, at least on the lower branch of the dispersion curve, is linearly polarized with the plane of polarization oriented at 90° to the wiggler magnetic field, as expected. The data for the upper branch exhibit more structure than could be obtained from a combination of plane waves propagating in the same direction. In general, the intensity pattern that would be expected from an arbitrarily polarized plane wave is given by an angular function of the form $P(\theta) = A + B\cos^2(\theta - \theta_o)$. Such regular behavior of the emitted laser beam is not observed, and it is likely that it is obscured by the coherent detection of scattered signals which reflect off the edges of the window of the vacuum system. The presence of a reproducible, though complicated, variation of intensity with angle indicates that the signal wave must still possess a significant degree of polarization.

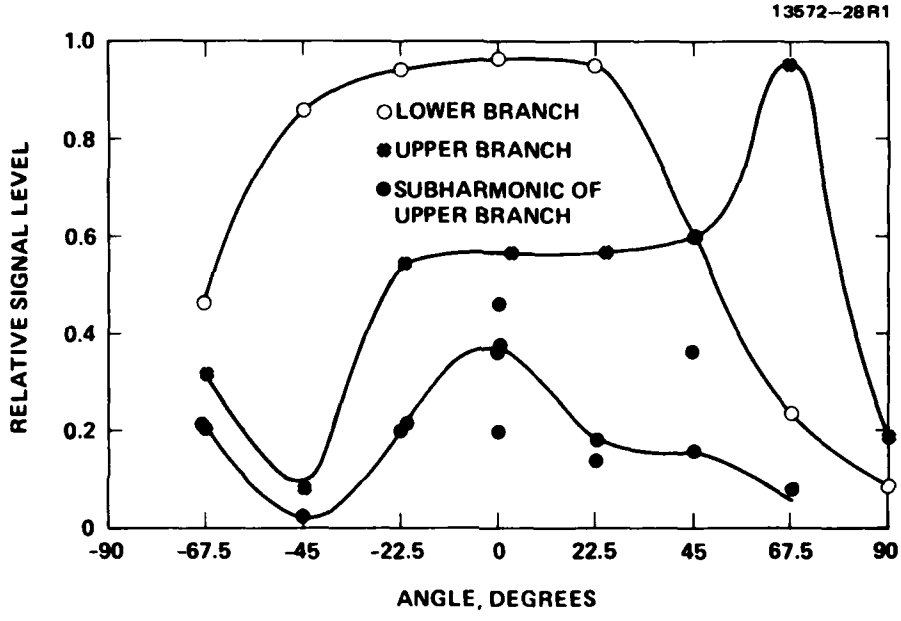

Figure 27. Polarization of FEL output radiation.

SECTION 5

SUMMARY OF EXPERIMENTAL RESULTS

Preliminary, first-stage FEL experiments have been carried out which have lead to the demonstration of the first plane-polarized mm-wave FEL oscillator operating in the K_a-band at 31 GHz with an output power of 60 kW and a generated power of 120 kW. These power values correspond to a laser efficiency of 4.1% which is consistent with an efficiency determined by the gain-bandwidth of the system. The signal duration can be made to extend beyond 10 μs if the voltage is held constant to within about 1% of the voltage needed to produce that frequency (at the high-Q resonance of the oscillator cavity).

The small signal gain of the system under lasing conditions has been determined to be around 5% for both the forward- and backward-wave branches of the dispersion curve. This is below the theoretically expected gain, but this may be explained by non-ideal propagation of the E-beam through the resonator, which was experienced during testing.

The frequency distribution agrees with the theoretical dispersion curves and with resonator design. The polarization appears to be linear and in the expected orientation. Frequency (or equivalently, voltage) pulling due to laser saturation, betatron motion and FEL action is observed; these effects follow theoretical estimates. Harmonic generation due to both the forward- and backward-wave operation has also been observed.

REFERENCES

1. F.A. Dolezal, H.E. Gallagher, R.J. Harvey, A.J. Palmer and C.G. Parazzoli, "Towards A Two-Stage Free Electron Laser," Presented at ONR Workshop on Free Electron Lasers, Sun Valley, Idaho, June 22-25, 1981.

2. D. Prosnitz, "Infrared and Visible Free Electron Lasers," in Handbook of Laser Science and Technology, (CRC Press, Inc., 1982).

3. L.R. Elias, "High-Power, cw, Efficient, Tunable(uv through ir) Free-Electron Laser Using Low-Energy Electron Beams," Phys. Rev. Let. 42, 977-980 (1979).

4. F.A. Dolezal, R.J. Harvey, and C.G. Parazzoli, "E-guns and Depressed Collectors for Two-Stage Free Electron Lasers," IEEE J. of Quan. Elect. QE-19, 309-315 (1983).

5. F.A. Dolezal, R.J. Harvey, A.J. Palmer, and C.G. Parazzoli, "Experimental Investigation of the Free Electron Laser," Hughes Aircraft Co. Final Report for Contract No. N00014-79-C-0957, Feb. 1982.

6. W.B. Herrmannsfeldt, "Poisson Equation Solving Program," Stanford Linear Accelerator Center Report No. SLAC-226, 1979.

7. J.A. Pasour, C.W. Roberson and F. Mako, NRL Memorandum Rep. 4791, June, 1982.

8. R.L. Abrams, "Coupling Losses in Hollow Waveguide Laser Resonators," IEEE J. Quan. Elect. QE-8, 838-843 (1972).

9. A. Hasegawa, "Free Electron Laser," Bell System Tech. J. 57, 3069-3089 (1978).

END

FILMED

6-85

DTIC